FEBS Letters

Real-time detection of central carbon metabolism in living *Escherichia coli* and its response to perturbations

Sebastian Meier [a,*], Pernille R. Jensen [b], Jens Ø. Duus [a,*]

[a] *Carlsberg Laboratory, Gamle Carlsberg Vej 10, 1799 Copenhagen, Denmark*
[b] *Albeda Research, Gamle Carlsberg Vej 10, 1799 Copenhagen, Denmark*

ARTICLE INFO

ABSTRACT

The direct tracking of cellular reactions in vivo has been facilitated with recent technologies that strongly enhance NMR signals in substrates of interest. This methodology can be used to assay intracellular reactions that occur within seconds to few minutes, as the NMR signal enhancement typically fades on this time scale. Here, we show that the enhancement of ^{13}C nuclear spin polarization in deuterated glucose allows to directly follow the flux of glucose signal through rather extended reaction networks of central carbon metabolism in living *Escherichia coli*. Alterations in central carbon metabolism depending on the growth phase or upon chemical perturbations are visualized with minimal data processing by instantaneous observation of cellular reactions.
© 2011 Federation of European Biochemical Societies. Published by Elsevier B.V. All rights reserved.

1. Introduction

Non-disruptive in vivo characterization of the cellular reaction machinery at work presents a timely challenge for chemical analysis and for post-genomic biology. The challenge consists in the sensitive spectroscopic detection of molecules of interest in presence of complex cellular backgrounds. In addition, direct detection of intracellular reactions is arguably best conducted with the natural substrates in absence of labeling groups that are introduced by chemical modification. These prerequisites are principally met by nuclear magnetic resonance (NMR) spectroscopy, which can employ natural substrates and resolve spectral signals of substrate and product in vivo [1].

Rather recently, methods that increase the orientation of nuclear magnetic moments (the spin polarization) $\sim 10^4$-fold in a substrate of choice have become popular, as these methods provide a means to enhance in vivo NMR signals of metabolites by several orders of magnitude [2]. Approaches for nuclear spin polarization enhancement (also called hyperpolarization) have the double benefit to increase signals of interest relative to the spectral noise and relative to non-enhanced backgrounds. These techniques thus specifically assay selected chemical reactions with a tracer of choice in vivo and complement popular metabolomics approaches for the comprehensive analysis of all intra- and extracellular low molecular weight metabolites ex vivo [3].

Spin polarization enhanced substrates have primarily been used for real-time ^{13}C NMR assays that monitor enzymatic transformations in mammalian systems [4–13]. Genetically and biologically more facile model organisms, on the other hand, have received minimal attention despite their key role in deciphering intact biological systems by probing responses to various biological, chemical and genetic perturbations [14]. We have recently shown that hyperpolarized dietary substrates can be tracked along entire metabolic pathways from substrate to metabolic end product in living *Saccharomyces cerevisiae* owing to its high glycolytic activity [15]. Encouraged by this finding, the current study aimed at establishing fast and background free in vivo visualizations of metabolic network plasticity in the metabolically more flexible model prokaryote *Escherichia*

Abbreviations: 1,3BPG, 1,3 bisphosphoglycerate; 2PG, 2-phosphoglycerate; 2,4 DNP, 2,4 dinitrophenol; 3PG, 3-phosphoglycerate; 6-PG, 6-phosphogluconate; 6-PGL, 6-phospho-δ-gluconolactone; AAT, alanine aminotransferase; Ac, acetate; Ac-CoA, acetyl-CoA; ACK, acetyl kinase; ADH, alcohol dehydrogenase; ALD, aldolase; DHAP, dihydroxyacetone phosphate; ENO, enolase; Frc-1,6P₂, fructose-1, 6-bisphosphate; Frc-6P, fructose-6phosphate; G6PDH, glucose-6phosphate dehydrogenase; GA3P, glyceraldehyde 3-phosphate; GAPDH, glyceraldehydes-3-phosphate dehydrogenase; Glc, glucose; Glc-6P, glucose-6phosphate; LB, lysogeny broth; LDH, lactate dehydrogenase; PDC, pyruvate decarboxylase; PDH E1/E2, pyruvate dehydrogenase components E1 and E2; PEP, phosphoenolpyruvate; PFK, phosphofructokinase; PFL, pyruvate formate lyase; PGD, 6-phosphogluconate dehydrogenase; PGL, 6-phosphogluconate lactonase; PGK, phosphoglycerate kinase; PGM, phosphoglycerate mutase; PTA, phosphotransacetylase; PTS, glucose-specific enzyme II of the phosphotransferase system; Pyr, pyruvate; PYK, pyruvate kinase; TPI, triosephosphate isomerase; YPD, yeast peptone dextrose

* Corresponding authors.

E-mail addresses: sebastian.meier@carlsberglab.dk (S. Meier), jens.duus@carlsberglab.dk (J.Ø. Duus).

Fig. 1. Overview of glycolysis, pentose phosphate pathway and mixed acid fermentation in *E. coli*. Reactions that are followed in real time in living *E. coli* BL21 are displayed.

coli. E. coli is known to modulate its metabolism at various catabolic branch points in response, e.g., to aeration, growth rate or oxidative and chemical stress [16,17]. Such adjustments of *E. coli* to varying growth phases and chemical perturbations are tracked by fast and easy-to interpret in vivo assays of the reaction network shown in Fig. 1.

2. Materials and methods

2.1. Cell culture

Precultures of the sequenced *E. coli* B strain BL21 [18] were inoculated in 20 ml lysogeny broth (LB) medium from agar plate and were grown over night at 37 °C at 200 rpm shaker speed. Shake flask cultures were inoculated from these precultures to $OD^{600} = 0.02$. Cells were grown to mid-exponential ($OD^{600} = 1$), late exponential ($OD^{600} = 3$) or stationary phase ($OD^{600} = 5$) at 200 rpm shaker speed. All mid-exponential cells and 70 ml both of the late exponential and of the stationary culture were harvested by centrifugation for 5 min at $15\,000 \times g$. Supernatants were discarded and the cell pellets were resuspended in 1.7 ml of 40 mM HEPES buffer of pH 7.3 containing 100 mg/l EDTA. Resuspended cells were transferred to a 10 mm NMR tube and were thermally equilibrated for 5 min prior to injection of hyperpolarized glucose. To a shake flask culture with late exponential cells ($OD^{600} = 3$), 1 mM 2,4-dinitrophenol was added prior to incubation at 37 °C for 45 min. Cells were harvested as described above and resuspended in 40 mM HEPES of pH 7.3 buffer containing 1 mM 2,4-dinitrophenol.

Precultures of *S. cerevisiae* BY4743 were inoculated to $OD^{600} = 0.1$ in YPD medium and were grown in shake flask culture to $OD^{600} = 0.8$ at 30 °C and 200 rpm shaker speed. Cells were harvested by centrifugation at $6000 \times g$ and were resuspended in fresh YP medium. Bacterial and yeast cells were resuspended into medium without glucose, as added carbon source in the medium would compete with hyperpolarized glucose fed for in vivo assays. In vivo assays with *S. cerevisiae* showed less pronounced metabolic adaptations than in *E. coli*.

2.2. Substrate and materials for hyperpolarization

Uniformly $^2H/^{13}C$-labeled glucose ([U-^{2}H, U-^{13}C]glucose) was chosen as substrate in order to provide non-protonated ^{13}C nuclei with sufficiently long hyperpolarization life time. Sufficient cellular uptake of the hyperpolarized substrate is an obvious prerequisite for conducting in vivo assays. *E. coli* glucose permease has a submillimolar Michaelis Menten constant towards glucose [19]. In vivo assays of glucose metabolism by *E. coli* were therefore conducted by injection of 2 mM substrate in order to saturate glucose transport by the permease. At this substrate concentration, the in vivo assay of *E. coli* consumes 8 mg of [U-^{2}H, U-^{13}C]glucose and thus is relatively inexpensive.

Nuclear spin polarization enhancement by dynamic nuclear polarization was conducted by dissolving 42 µmol (8 mg) of [U-^{2}H, U-^{13}C]glucose (Sigma Aldrich, St. Louis, MO) in 10 mg of aqueous polarization medium containing 27 mM trityl radical OX063 (Oxford Instruments, UK) and 0.9 mM trimeric Gd chelate of 1,3,5-tris-(N-(DO3A-acetamido)-N-methyl-4-amino-2-methyl-phenyl)-[1,3,5]tria-zinane-2,4,6-trione (GE Healthcare, Amersham, UK). Samples were vitrified by flash freezing in liquid helium inside a dedicated polarizer of 3.35 T magnetic field. Glucose solutions vitrify readily and yield amorphous frozen solutions that allow effective transfer of electron spin polarization to glucose nuclear spins.

2.3. Hyperpolarization and in vivo NMR

Microwave-driven polarization enhancement was performed by irradiation at 93.89 GHz and 100 mW for 50 min at 1.2 K. Samples were dissolved in 4.2 ml Milli-Q water containing 100 mg/l EDTA to yield liquid samples of 10 mM [U-^{2}H, U-^{13}C]glucose. To this end, the dissolution medium was pressurized to 4 bar and subsequently heated to 10 bar pressure. Hyperpolarized [U-^{2}H, U-^{13}C]glucose prepared in this manner reaches the bacterial cell suspension with a temperature near 37 °C. Cell suspensions were residing inside a 600 MHz NMR spectrometer and data acquisition was started prior to substrate injection in order to minimize experimental dead time see, e.g., Fig. 3.

Forceful injection by hand was used in order to ensure mixing of cell suspensions and substrate solutions inside the magnetic field. To this end, 600 µl of 10 mM [U-^{2}H, U-^{13}C]glucose solution were manually injected into 2.4 ml of *E. coli* cell suspension. The final substrate concentration was thus 2 mM glucose.

2.4. Data acquisition and processing

NMR spectra were recorded on a Bruker DRX 600 spectrometer equipped with a 10 mm room temperature probe head. ^{13}C NMR spectra were recorded as an array of 512 one-dimensional spectra using 6° flip angles (2 µs pulses). No decoupling was applied during data acquisition. A one-dimensional spectrum was recorded every 500 ms as two transients recorded for 170 ms each, prior to a 160 ms delay. Summation of two transients improves the signal to noise ratio of the resultant spectra at the cost of lower time resolution, which seemed acceptable considering that glycolysis and fermentations proceed on the >1 s timescale see, e.g., Fig. 3. 16384 data points were sampled in the time domain. Spectra were processed with an exponential line broadening of 25 Hz and integrated in Topspin 2.1. Hyperpolarization of glucose carbons fades with a $T_1\{14.1\ T\} \approx 12$ s for $^{13}C_{1-5}$ and 10 s for $^{13}C_6$. Tracking of bacterial metabolism for 1–2 min is aided by the catabolic conversion of glucose to metabolites containing quaternary carbons, whose hyperpolarization fades slower than the substrate hyperpolarization. In order to account for possible variations in substrate polarization at the time of glucose injection, spectra were normalized using glucose signals.

3. Results and discussion

3.1. Pulse-response setup: In vivo tracking of central carbon metabolism

We attempt to visualize extended reaction networks of central carbon metabolism in vivo with a hyperpolarized dietary substrate (glucose in perdeuterated and uniformly ^{13}C-enriched form) substrate that is efficiently taken up and metabolized by the cell. [U-^{2}H, U-^{13}C]glucose polarized to ~25% in the solid state. After dissolution of the vitrified and hyperpolarized glucose sample, the substrate was mixed with an E. coli BL21 cell suspension residing in a 14.1 Tesla NMR spectrometer in order to detect chemical transformations of the substrate by living E. coli (Fig. 2A). This
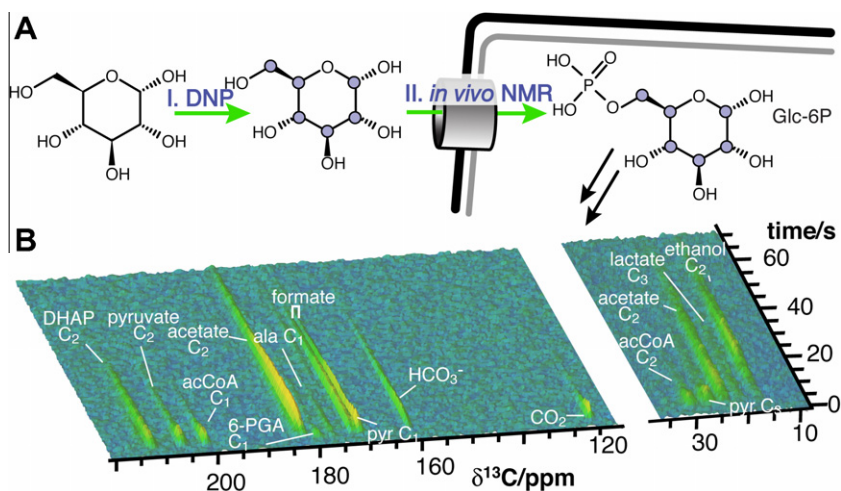
Fig. 2. (A) Instantaneous pulse-response measurements of microbial metabolism with a pulse of hyperpolarized [U-^{2}H, U-^{13}C]glucose fed to a cell suspension of E. coli BL21. Hyperpolarization of ^{13}C-enriched glucose enhances tracer signal ~10^6-fold over the natural background and thus allows pulse-response type experiments yielding only signals of the substrate and its metabolites. (B) Resultant time series of glucose metabolism by Escherichia coli as monitored by recording a ^{13}C NMR spectrum every 0.5 s. A time series of 150 one-dimensional spectra is shown. Time of substrate injection is defined as time zero. The overall signal decays as hyperpolarization fades. Formate signal is split by the $^1J^{CH}$ coupling as no proton decoupling is applied during acquisition of the ^{13}C spectra. Note that pyruvate C$_1$ signal overlaps with the split formate signal.
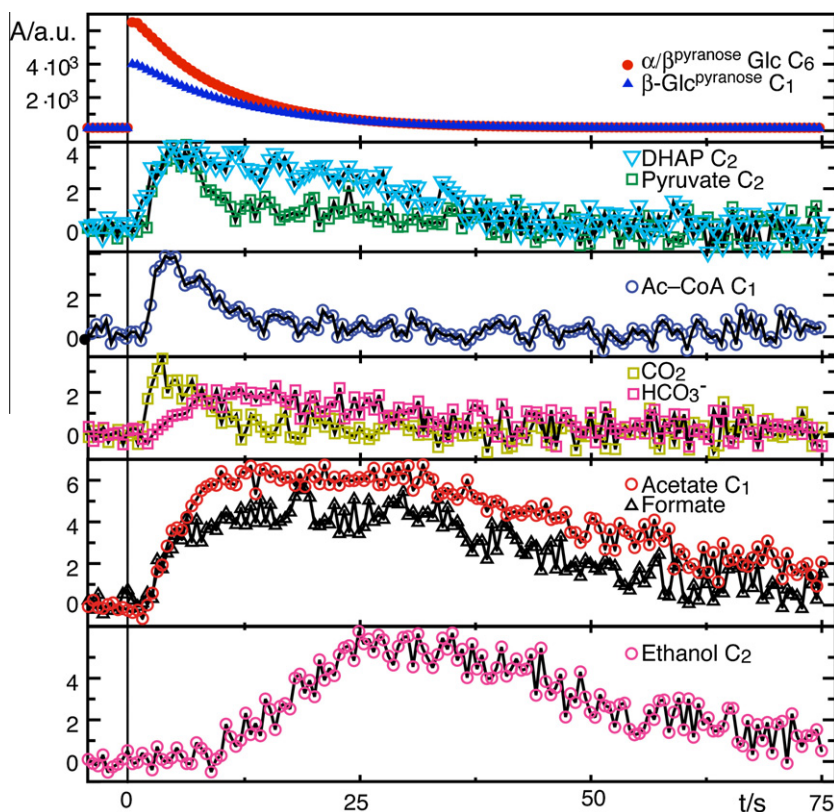
Fig. 3. Time series of substrate and metabolite signal areas in the experiment shown in Fig. 2B corrected for polarization losses from previous one-dimensional NMR spectra. Signals from major intermediates and products of glycolysis and fermentation are shown. Formate and ethanol C$_2$ are protonated by metabolism in aqueous medium. Formate signal area is taken as twice the area of the non-overlapping downfield doublet peak.

in vivo pulse-response setup yields a kinetic experiment as depicted in Fig. 2 upon feeding 2 mM hyperpolarized [U-^{2}H, U-^{13}C]glucose to *E. coli* BL21 cells at 37 °C. The conversion of glucose signal into several metabolic intermediates and products by reactions of Fig. 1 is directly detected in real-time and occurs within few seconds (Figs. 2 and 3).

Major metabolites that are quickly formed and yield signals that are resolved from the substrate and other metabolite signals include gluconate-6phosphate (6-PGA; C_1 179.1 ppm), fructose-1,6bisphosphate (C_2^{α} 105.3 ppm; C_2^{β} 101.7 ppm), dihydroxyacetonephosphate (DHAP; C_2 211.9 ppm), pyruvate (C_1 205.8 ppm; C_2 170.9 ppm; C_3 26.8 ppm), acetyl-CoA (C_1 201.3 ppm; C_2 30.4 ppm), lactate (C_1 182.9 ppm; C_2 20.3 ppm), alanine (C_1 176.4 ppm), acetate (C_1 181.9 ppm; C_2 23.4 ppm), formate (doublet at 171.6 ppm), CO_2 (125.2 ppm), HCO_3^- (bicarbonate; 160.6 ppm), ribulose-5P (C_2; 213.7 ppm) and ethanol (C_1 58.1 ppm; C_2 16.9 ppm) (Fig. 2B). As expected, DHAP is the first acyclic glycolytic keto-compound to appear. Pyruvate, CO_2 and acetyl-CoA signals build up within ~1 s after emergence of DHAP signal. DHAP, pyruvate, acetyl-CoA and CO_2 approach maximum signal levels within 5 s after glucose injection. Ethanol signal is formed considerably slower than signals of other detected metabolic end products such as bicarbonate, acetate or formate, which approach their maxima ~10 s after glucose injection. Signals decay due to the fading of hyperpolarization in substrate and metabolites and due to chemical turnover (Fig. 3).

Overall, entire metabolic pathways of glycolysis and mixed acid fermentation are visualized by real-time in vivo spectroscopy at physiological temperatures in living *E. coli* BL21. Formation of acetate, formate, bicarbonate, CO_2 and ethanol from glucose substrate results from at least ten enzyme-catalyzed transformations in living *E. coli* (Fig. 1). The possibility to directly assay multistep reactions from substrate to product, including the time-resolved detection of intermediate signals (Figs. 2B and 3), within seconds of experiment time emphasizes the enzymatic efficiency of microbial glucose catabolism and the power of spin polarization enhanced NMR to directly assay entire pathways in single experiments.

3.2. Adaptation to nutritional changes

Bacteria have to be able to rapidly adapt their metabolism to prevailing conditions, e.g., when they deplete the growth medium for nutrients and oxygen [20]. We therefore set out to detect metabolic adaptations in shake flask cultures of *E. coli* BL21 at different growth phases (Fig. 4). Resultant experiments differ most prominently in a metabolite signal at 175 ppm. This signal is ascribed to δ-6-phosphogluconolactone due to its chemical shift and early emergence in parallel to gluconate-6 phosphate. Conversion of glucose to δ-6-phosphogluconolactone is roughly fivefold higher in exponentially growing ($OD^{600} = 1$) than in stationary ($OD^{600} = 5$) cells (Fig. 4).

Formation of δ-6-phosphogluconolactone by the glucose 6-phosphate dehydrogenase catalyzed reaction is the first reaction in the oxidative branch of the pentose phosphate pathway. Glucose 6-phosphate dehydrogenase (encoded by the *zwf* gene) is subject to growth-rate-dependent control [16] and enzyme levels of glucose-6-phosphate dehydrogenase in cellular extracts increase three- to fivefold with increasing growth rate [21] due to transcriptional activation of the *zwf* gene [16]. Increased in vivo formation of δ-6-phosphogluconolactone from hyperpolarized glucose tracer during mid-exponential growth thus agrees well with levels of transcriptional activation of the *zwf* gene at increasing growth rate and with increased demand for reductive biosynthesis. On the other hand, flux of hyperpolarized glucose signal into acetate and formate pools in shake-flask LB cultures of *E. coli* BL21 is slightly
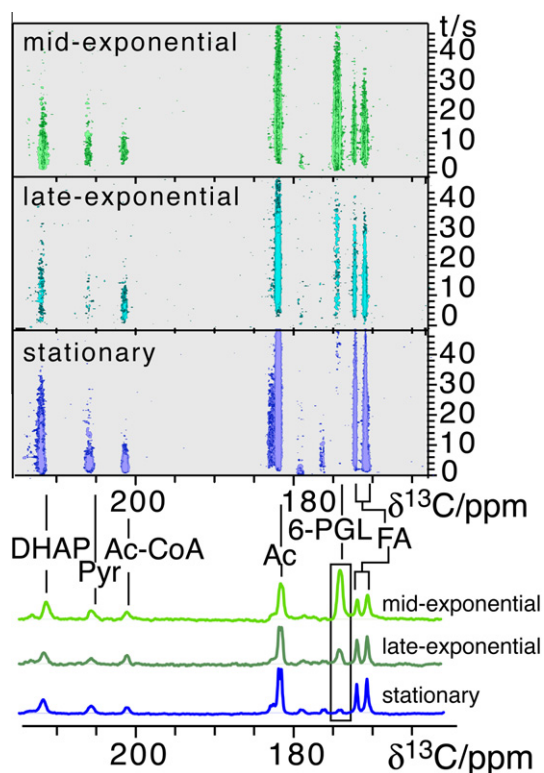

Fig. 4. Growth-phase dependent metabolic adjustment in *E. coli*. 6-PGL formation by glucose-6 phosphate dehydrogenase – a growth rate dependent enzyme – decreases as cells decelerate growth (top, time course; bottom, sum signal during the first 50 s of the kinetic experiment shown on top).

increased at higher cell density, presumably due to increasingly anaerobic conditions [22]. Overall, the formation of intermediates and products of glycolysis and fermentation is less affected by growth phase (Fig. 4) than δ-6-phosphogluconolactone formation.

3.3. Response to protonophore

Besides being subject to growth-rate dependent regulation, the *zwf* gene encoding glucose 6-phosphate dehydrogenase is a member of the multiple antibiotic resistance (*mar*) operon and is transcriptionally induced by various antibiotics and aromatic acids [16,23,24]. 2,4-Dinitrophenol is a particularly strong inducer of the *mar* promoter at low (~1 mM) amounts and was accordingly used for chemical perturbation of *E. coli* BL21 cells. Late exponential ($OD^{600} = 3$) *E. coli* BL21 was challenged for 45 min with 1.0 mM of 2,4-dinitrophenol (Fig. 5). In vivo spectroscopy of *E. coli* BL21 glucose metabolism in presence of 2,4-dinitrophenol yields a dominant signal of the δ-6-phosphogluconolactone (6-PGL) reflecting even higher reaction usage than during exponential growth, while hydrolysis of the δ-6-phosphogluconolactone is the bottleneck for the oxidative pentose phosphate pathway in *E. coli* BL21 under these conditions (Fig. 5).

Multiple changes to glucose catabolism in presence of 2,4-dinitrophenol are evident (Fig. 5), as chemical uncouplers affect the cellular redox and energy charge and will impact on reactions by modulating the concentrations of cofactors and allosteric regulators. Specifically, flux of tracer signal into ethanol and formate pools are significantly reduced, while pyruvate and CO_2/bicarbonate formation are increased. Formate and ethanol formation (and secretion) are means for regulating cellular redox balance by eliminating surplus redox equivalents [22]. 2,4-Dinitrophenol supposedly reduces the need to eliminate redox equivalents by reducing the cellular reductive power [25].
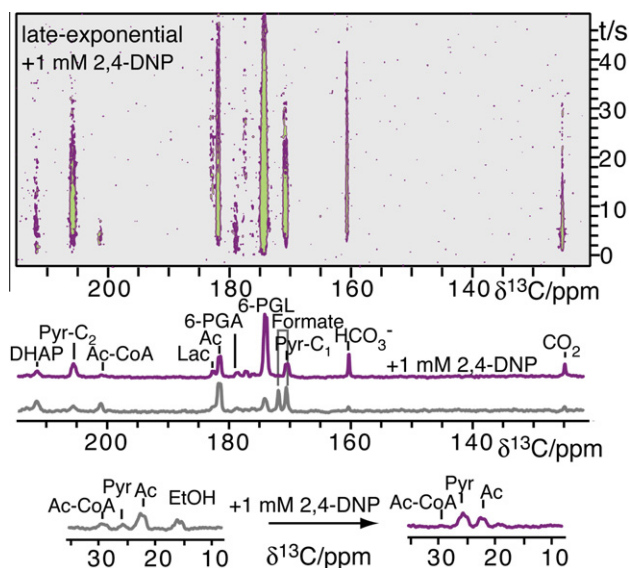
Fig. 5. Alterations to cellular biochemistry upon adding 1 mM 2,4-dintrophenol at 37 °C to late exponential cells (see Fig. 4). Formate and ethanol signals vanish, while pyruvate and 6-PGL accumulate and CO_2/bicarbonate formation is strongly enhanced. The carbonyl (top and middle) and methyl regions of the ^{13}C spectra are shown (top, time course; bottom, sum signal during the first 50 s of the kinetic experiment shown on top).

Reduced usage of the pyruvate formate lyase and pyruvate decarboxylase catalyzed reactions agrees with the increased accumulation of pyruvate (Fig. 5) in presence of 2,4-dinitrophenol. CO_2 is formed by several of the assayed reactions (Fig. 1) and the fast formation of increased CO_2 levels in presence of uncoupler likely reflects increased oxidative decarboxylation of pyruvate and 6-phosphogluconate due to reduced reductive power. Such adaptations to chemical uncouplers may be relevant in natural habitats, where bacteria can encounter conditions that are mimicked by chemical uncouplers [26]. As instantaneous pulse-response experiments with hyperpolarized tracer do not require that cells thrive and multiply, the methodology is well suited for studying metabolic adaptations in response to extracellular perturbations, even if these perturbations are detrimental to cellular physiology.

3.4. Comparison of glucose metabolism in living E. coli and S. cerevisiae

Fig. 6 compares the time dependent redistribution of substrate signal into metabolic pathways of different organisms by visualizing the fate of glucose in pulse-response experiments on E. coli BL21 and
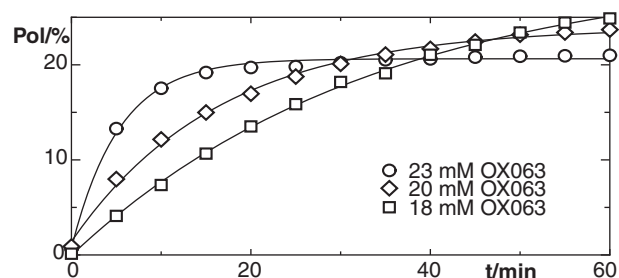
Fig. 7. Buildup of ^{13}C net spin orientation (polarization) in [U-^2H, U-^{13}C]glucose in dependence of sample composition. 8 mg of [U-^2H, U-^{13}C]glucose were dissolved in 9.5, 11.5 or 15 mg of aqueous polarization medium containing 27 mM trityl radical OX063 and 0.9 mM trimeric Gd chelate, resulting in solutions containing 18, 20 and 23 mM of the radical, respectively. More than 20% net spin orientation is achieved within 15 min at 23 mM radical concentration.

S. cerevisiae BY4743. E. coli and S. cerevisiae cell cultures were grown in the nutritionally rich media LB and YPD, respectively. In vivo assays of glucose turnover reflect the streamlining of S. cerevisiae metabolism for alcoholic fermentation to CO_2 and ethanol, as Saccharomyces out-competes other microorganisms in natural habitats by producing ethanol [27]. Additional intermediates and additional metabolic products are detectable in E. coli BL21. Glycolysis, initial steps of the pentose phosphate pathway and fermentation proceed on the seconds timescale in E. coli and S. cerevisiae (Fig. 6).

Signal maxima of glycolytic intermediates emerge faster in E. coli than in S. cerevisiae. Bottlenecks of glycolysis and fermentation seem to be similar in both organisms, however. DHAP signal accumulates in both organisms within few seconds after feeding of glucose tracer, while the subsequent reaction intermediates GA-3P, 3-PG, 2-PG and PEP are low populated and not detected with the current setup. Signal from the subsequent pathway intermediate pyruvate is well detectable both in E. coli and S. cerevisiae. Pyruvate signal decays more rapidly in E. coli, however, presumably due to the faster clearance by alternative fermentation routes.

In these studies, the need to employ deuterated rather than protonated glucose may introduce kinetic isotope effects that could lead to an underestimation of metabolic kinetics. The use of deuterated substrate is expected to affect the rate of individual reaction steps, in particular bond-breaking dehydrogenations. Nevertheless, the timing of DHAP, pyruvate and ethanol signal formation from deuterated ^{13}C glucose and protonated 2-^{13}C fructose is very similar after feeding of these hyperpolarized sugars to living yeast [15]. This small isotope effect on metabolic kinetics could be a consequence of the multistep nature of metabolism and even of enzyme-catalyzed reactions themselves, where the bond-breaking steps may contribute weakly to kinetic control [28]. Comparing metabolic
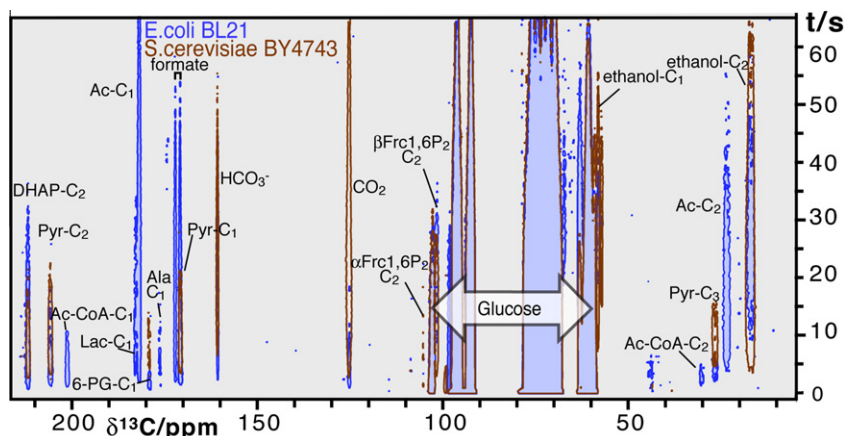

Fig. 6. Comparison of glucose metabolism in living E. coli BL21 (blue) and S. cerevisiae BY4743 (red) grown in rich media.

kinetics of non-deuterated and deuterated [2-^{13}C]ketoses or per-deuterated and partially deuterated aldoses could be a means to directly assay isotope effects in living metabolic pathways by hyperpolarized NMR.

4. Conclusion

Hyperpolarized NMR allows the real-time monitoring of rather extended reaction networks, if substantial substrate turnover occurs on the seconds timescale. The current study indicates the usefulness of hyperpolarized ^{13}C NMR for the real-time detection of changes to cellular biochemistry under defined genetic and nutritional conditions. Adaptations in central carbon metabolism of living *E. coli* BL21 to extracellular signals or perturbations are visualized by the direct detection of changes to the usage and timing of cellular reactions. The assay is compatible with the use of Good's buffers [29] as ^{13}C enrichment and hyperpolarization increase tracer signal ∼10^6-fold over the carbon signal from the non-hyperpolarized buffer.

The most time consuming step of the in vivo assay is the spin polarization enhancement of the [U-^{2}H, U-^{13}C]glucose tracer, which approaches levels of 30% net spin alignment with time constants on the order of 1000 s (Fig. 7). Changes to the spin polarization protocol can yield acceptable polarization at substantially reduced times (Fig. 6). A net spin alignment of 20% can be achieved in this manner with the current setup within 15 min polarization time, compared to 12×10^{-4}% alignment in the detecting 600 MHz NMR spectrometer at 37 °C in absence of polarization enhancement. Throughput could be further increased by parallel polarization and separate dissolution of samples in polarizers with several separate sample spaces [30]. Thus, the method yields direct information on cellular biochemistry at work by reasonably fast assays that do not require model dependent data interpretation.

Acknowledgement

References

[1] Grivet, J.-P. and Delort, A.-M. (2009) NMR for microbiology: in vivo and in situ applications. Prog. Nucl. Magn. Reson. Spectrosc. 54, 1–53.
[2] Ardenkjær-Larsen, J.H. et al. (2003) Increase in signal-to-noise ratio of >10,000 times in liquid-state NMR. Proc. Natl. Acad. Sci. USA 100, 10158–10163.
[3] Mashego, M.R., Rumbold, K., De Mey, M., Vandamme, E., Soetaert, W. and Heijnen, J.J. (2007) Microbial metabolomics: past, present and future methodologies. Biotechnol. Lett. 29, 1–16.
[4] Gallagher, F.A. et al. (2008) Magnetic resonance imaging of pH in vivo using hyperpolarized 13C-labelled bicarbonate. Nature 453, 940–943.
[5] Golman, K., Zandt, R.I., Lerche, M., Pehrson, R. and Ardenkjaer-Larsen, J.H. (2006) Metabolic imaging by hyperpolarized 13C magnetic resonance imaging for in vivo tumor diagnosis. Cancer Res. 66, 10855–10860.
[6] Schroeder, M.A. et al. (2009) Real-time assessment of Krebs cycle metabolism using hyperpolarized 13C magnetic resonance spectroscopy. FASEB J. 23, 2529–2538.
[7] Merritt, M.E., Harrison, C., Storey, C., Jeffrey, F.M., Sherry, A.D. and Malloy, C.R. (2007) Hyperpolarized 13C allows a direct measure of flux through a single enzyme-catalyzed step by NMR. Proc. Natl. Acad. Sci. USA 104, 19773–19777.
[8] Gallagher, F.A. et al. (2009) Production of hyperpolarized [1,4-13C2]malate from [1,4-13C2]fumarate is a marker of cell necrosis and treatment response in tumors. Proc. Natl. Acad. Sci. USA 106, 19801–19806.
[9] Schroeder, M.A., Cochlin, L.E., Heather, L.C., Clarke, K., Radda, G.K. and Tyler, D.J. (2008) In vivo assessment of pyruvate dehydrogenase flux in the heart using hyperpolarized carbon-13 magnetic resonance. Proc. Natl. Acad. Sci. USA 105, 12051–12056.
[10] Keshari, K.R. et al. (2009) Hyperpolarized [2-13C]-fructose: a hemiketal DNP substrate for in vivo metabolic imaging. J. Am. Chem. Soc. 131, 17591–17596.
[11] Chen, A.P. et al. (2008) Feasibility of using hyperpolarized [1-13C]lactate as a substrate for in vivo metabolic 13C MRSI studies. Magn. Reson. Imaging 26, 721–726.
[12] Jensen, P.R., Karlsson, M., Meier, S., Duus, J.O. and Lerche, M.H. (2009) Hyperpolarized amino acids for in vivo assays of transaminase activity. Chemistry 15, 10010–10012.
[13] Jensen, P.R., Peitersen, T., Karlsson, M., In't Zandt, R., Gisselsson, A., Hansson, G., Meier, S. and Lerche, M.H. (2009) Tissue-specific short chain fatty acid metabolism and slow metabolic recovery after ischemia from hyperpolarized NMR in vivo. J. Biol. Chem. 284, 36077–36082.
[14] Ideker, T., Galitski, T. and Hood, L. (2001) A new approach to decoding life: systems biology. Annu. Rev. Genomics Hum. Genet. 2, 343–372.
[15] Meier, S., Jensen, P. R. and Duus, J. O. (2011) Metabolic pathway visualization in living yeast by DNP-NMR. Mol. BioSyst. DOI:10.1039/C1MB05202K.
[16] Fawcett, W.P. and Wolf Jr., R.E. (1995) Genetic definition of the Escherichia coli zwf "soxbox", the DNA binding site for SoxS-mediated induction of glucose 6-phosphate dehydrogenase in response to superoxide. J. Bacteriol. 177, 1742–1750.
[17] Alexeeva, S., de Kort, B., Sawers, G., Hellingwerf, K.J. and de Mattos, M.J. (2000) Effects of limited aeration and of the ArcAB system on intermediary pyruvate catabolism in Escherichia coli. J. Bacteriol. 182, 4934–4940.
[18] Jeong, H. et al. (2009) Genome sequences of Escherichia coli B strains REL606 and BL21(DE3). J. Mol. Biol. 394, 644–652.
[19] Nuoffer, C., Zanolari, B. and Erni, B. (1988) Glucose permease of Escherichia coli. The effect of cysteine to serine mutations on the function, stability, and regulation of transport and phosphorylation. J. Biol. Chem. 263, 6647–6655.
[20] Wolfe, A.J. (2005) The acetate switch. Microbiol. Mol. Biol. Rev. 69, 12–50.
[21] Wolf Jr., R.E., Prather, D.M. and Shea, F.M. (1979) Growth-rate-dependent alteration of 6-phosphogluconate dehydrogenase and glucose 6-phosphate dehydrogenase levels in Escherichia coli K-12. J. Bacteriol. 139, 1093–1096.
[22] Varma, A., Boesch, B.W. and Palsson, B.O. (1993) Stoichiometric interpretation of Escherichia coli glucose catabolism under various oxygenation rates. Appl. Environ. Microbiol. 59, 2465–2473.
[23] Scott, D.B. (1956) The oxidative pathway of carbohydrate metabolism in Escherichia coli. 4. Formation of enzymes induced by 2:4-dinitrophenol. Biochem. J. 63, 593–600.
[24] Cohen, S.P., Levy, S.B., Foulds, J. and Rosner, J.L. (1993) Salicylate induction of antibiotic resistance in Escherichia coli: activation of the mar operon and a mar-independent pathway. J. Bacteriol. 175, 7856–7862.
[25] Boshoff, H.I., Myers, T.G., Copp, B.R., McNeil, M.R., Wilson, M.A. and Barry 3rd, C.E. (2004) The transcriptional responses of Mycobacterium tuberculosis to inhibitors of metabolism: novel insights into drug mechanisms of action. J. Biol. Chem. 279, 40174–40184.
[26] Gage, D.J. and Neidhardt, F.C. (1993) Adaptation of Escherichia coli to the uncoupler of oxidative phosphorylation 2, 4-dinitrophenol. J. Bacteriol. 175, 7105–7108.
[27] Rozpedowska, E. et al. (2011) Parallel evolution of the make-accumulate-consume strategy in Saccharomyces and Dekkera yeasts. Nat. Commun. 2, 302.
[28] Hermes, J.D., Roeske, C.A., O'Leary, M.H. and Cleland, W.W. (1982) Use of multiple isotope effects to determine enzyme mechanisms and intrinsic isotope effects. Malic enzyme and glucose-6-phosphate dehydrogenase. Biochemistry 21, 5106–5114.
[29] Good, N.E., Winget, G.D., Winter, W., Connolly, T.N., Izawa, S. and Singh, R.M. (1966) Hydrogen ion buffers for biological research. Biochemistry 5, 467–477.
[30] Ardenkjaer-Larsen, J.H., Urbahn, J., Leach, A., Stautner, E., Zhang, T. and Clarke, N. (2009) A closed helium sorption pump system and its use in hyperpolarized 13C metabolic imaging. In: 2nd DNP Symposium, Königstein, 38.